[11] Pok, D., Chen, C., Schamus, J., Montgomery, C., and Tsui, J.
Chip design for monobit receiver.
IEEE Transactions on Microwave Theory and Techniques, **45** (Dec. 1997).

[12] Grajal, J., Blázquez, R., López-Risueño, G., Sanz, J. M., Burgos, M., and Asensio, A.
Analysis and characterisation of a monobit receiver for electronic warfare.
IEEE Transactions on Aerospace and Electronic Systems, **39**, 1 (Jan. 2003).

[13] Sanchez, M., Garrido, M., López-Vallejo, M., and López-Barrio, C.
Automated design space exploration of FPGA-based FFT architectures based on area and power estimation.
In *Proceedings of IEEE International Conference on Field Programmable Technology* (FPT 2006), 2006, 127–134.

[14] Yun-Nan, C., and Parhi, K.
An efficient pipelined FFT architecture.
IEEE Transactions on Circuits and Systems II, **50**, 6 (2003), 322–325.

[15] Sansaloni, T., Pérez-Pascual, A., and Valls, J.
Area-efficient FPGA-based FFT processor.
Electronics Letters, **39**, 19 (2003).

[16] Szedo, G., Yang, V., and Dick, C.
High-performance FFT processing using reconfigurable logic.
In *35 Asilomar Conference on Signals, Systems and Computers*, 2001, 1353–1356.

[17] Cooley, J. W., and Tukey, J. W.
An algorithm for machine calculation of complex Fourier series.
Mathematics of Computation, **19** (1965).

[18] Volder, J. E.
The CORDIC trogonometric computing technique.
IRE Transactions on Electronic Computing, (1959).

[19] Jun, W., Shiyi, M., and Yuezhong, W.
Design and implementation of a high speed vector processor for real-time SAR imaging.
In *Proceedings of CIE International Conference on Radar*, 2001.

[20] Xilinx Inc.
Xilinx LogiCore: Fast Fourier Transform v3.1, 2004.
http://www.xilinx.com/products/Broadband/.

[21] Nordin, G., Milder, P. A., Hoe, J. C., and Püschel, M.
Automatic generation of customized discrete Fourier transform IPs.
In *Proceedings of Design Automation Conference* (DAC), 2005.

[22] Li, F., Chen, D., He, L., and Cong, J.
Architecture evaluation for power-efficient FPGAs.
In *Proceedings of ACM International Symposium on Field Programmable Gate Arrays*, 2003, 175–184.

[23] Curd, D.
Power consumption in 65 nm FPGAs, 2006, white paper: Virtex-5 Family of FPGAs.
http://www.xilinx.com.

[24] Skolnik, M. I.
Introduction to Radar Systems (3rd ed.).
New York: McGraw-Hill, 2001.

[25] Harris, F. J.
On the use of windows for harmonic analysis with the discrete Fourier transform.
Proceedings of the IEEE, **66**, 1 (Jan. 1978), 51–83.

[26] López-Risueño, G., Grajal, J., and Sanz-Osorio, A.
Digital channelized receiver based on time-frequency analysis for signal interception.
IEEE Transactions on Aerospace and Electronic Systems, **41**, 3 (July 2005).

[27] ATMEL Corporation
Broadband Data Conversion Products, 2005.
http://www.atmel.com/products/Broadband/.

Wideband DOA Estimation Algorithms for Multiple Moving Sources using Unattended Acoustic Sensors

The problem of direction of arrival (DOA) estimation for multiple wideband sources using unattended passive acoustic sensors is considered. Several existing methods for narrowband DOA estimation are extended to resolve multiple closely spaced sources in presence of interference and wind noise. New wideband Capon beamforming methods are developed that use various algorithms for combining the narrowband power spectra at different frequency bins. A robust wideband Capon method is also studied to account for the inherent uncertainties in the array steering vector. Finally, to improve the resolution within an angular sector of interest and to provide robustness to sensor data loss, the beamspace method is extended and applied to the wideband problems. These methods are tested and benchmarked on two real acoustic signature data sets that contain multiple ground vehicles.

I. INTRODUCTION

The problem of detection, and localization of multiple ground targets using unattended acoustic sensors is complicated due to various factors. These include: variability and nonstationarity of source acoustic signatures, signal attenuation and fading effects as a function of range and Doppler, coherence loss due to environmental conditions and wind effects, near field and nonplane wave effects, and high level of acoustic clutter and interference. In addition, presence of multiple closely spaced targets that move in tight formations, e.g. staggered, abreast or single-file, further complicates the direction of arrival (DOA) estimation, data association, and localization processes. Clearly, optimum performance for detection and localization of multiple acoustic sources is

Manuscript received May 30, 2007; revised February 6, 2008; released for publication April 3, 2008.

IEEE Log No. T-AES/44/4/930741.

Refereeing of this contribution was handled by B. LaScala.

This work was funded by Army SBIR-Phase II Contract DAAE30-03-C-1055. The first data set was provided by the U.S. Army ARDEC, Picatinny Arsenal. The second data set was collected by Information System Technologies, Inc.

highly dependent on terrain, weather, and background noise.

To date, several wideband DOA estimation algorithms [1–3] for resolving moving ground targets from their acoustic signatures have been developed. These algorithms mainly involve sensor array processing that apply to baseline or regular (e.g. linear or circular) array geometries. Wideband extensions (coherent and incoherent) of the MUSIC (multiple signal classification) algorithm [4] are among the techniques that have shown promise for resolving multiple moving ground vehicles. In particular, the advantage of wideband MUSIC over the delay-sum algorithm was demonstrated in [2], via experimental results obtained from a circular array of six sensors, with a diameter of 8 ft. In [3], several wideband DOA estimation methods including steered covariance matrix (STCM) [5, 6] and spatial smoothing or array manifold interpolation [5] have been employed for DOA tracking of ground vehicles. In addition, experimental analysis of DOA estimation accuracy of the incoherent and coherent wideband MUSIC algorithms have been provided. The results presented in [3] indicate that incoherent wideband methods yield more accurate DOA estimates for highly peaked spectra while for sources with flat spectra the coherent wideband methods generate more accurate DOA estimates.

In [7], an algorithm for DOA tracking of multiple ground vehicles which move in a single-file convoy is developed. The proposed algorithm uses a template for the DOA track of the leading vehicle to generate DOA tracks for the remaining vehicles. DOA estimates are generated using the incoherent wideband MUSIC. This method also utilizes the differential estimates in vehicles' speeds to obtain more accurate DOA estimates for each vehicle in the convoy. Heuristic rules are used to build the templates of the leading and trailing vehicles. The work in [8] uses an adaptive beamforming algorithm at a fixed look angle with enhanced directivity and reduced sidelobes. Using this algorithm the number of targets in a convoy can also be determined.

More recently, a study was carried out [9] to benchmark different wideband DOA estimation algorithms. Among the methods carefully studied were the STCM [6] and the weighted subspace fitting (WSF) [4, 10]. The STCM typically uses a diagonal focusing matrix, which can resolve a group of sources only if all the DOAs are within one beamwidth of the focusing angle. Other choices of the focusing matrix [11] were also found to be incapable of providing accurate DOA estimates of multiple closely spaced sources. The WSF method requires a multi-dimensional search for determining the DOAs, and hence is computationally inefficient for practical use.

This paper presents three new wideband DOA estimation algorithms for resolving ground vehicles moving in tight formations. These algorithms are based on wideband extensions of the narrowband Capon beamformer [4]. The proposed methods exploit the arithmetic mean, geometric mean, and harmonic mean of the output angular power of narrowband Capon beamformers at different frequency bins for wideband DOA estimation. The proposed algorithms are combined with the robust Capon beamformer presented in [12] to improve the robustness of the DOA estimates with respect to steering vector errors and wavefront perturbations. The beamspace method [4] is also integrated with the wideband Capon methods in order to further enhance the DOA estimation resolution and provide robustness to sensor loss. An analysis of the bearing response patterns of wideband Capon beamformers is performed to investigate the ability of these beamformers to resolve multiple closely spaced sources. These algorithms are then tested and benchmarked on two real acoustic signature data sets. The first data set was collected using baseline circular arrays of five microphones and contains acoustic signatures of multiple light or heavy, wheeled or tracked vehicles. This data set is used to demonstrate the usefulness of the proposed methods for resolving multiple closely spaced targets. The second data set was collected using distributed wireless acoustic sensors and contains acoustic signatures of one or two light wheeled vehicles. This data set is used to show the promise of the wideband beamspace method in presence of sensor failures.

II. WIDEBAND SIGNAL MODEL

Consider an array of M sensors that receive the wavefield emanated from d wideband sources in presence of noise. The array geometry is arbitrary but known to the processor. The source signal vector $\mathbf{s}(t) = [s_1(t), s_2(t), \ldots, s_d(t)]^T$ is assumed to be zero mean and stationary over the observation interval T_0. The source spectral density matrix is denoted by $\mathrm{P}_{\mathbf{s}}(f)$, $f \in [f_c - BW/2, f_c + BW/2]$, where the bandwidth BW is comparable to center frequency f_c. The spectral density matrix $\mathrm{P}_{\mathbf{s}}(f)$ is a $d \times d$ nonnegative Hermitian matrix, which is unknown to the processor. The noise wavefield is assumed to be independent of the source signals, with $M \times M$ noise spectral density matrix $\mathrm{P}_{\mathbf{n}}(f)$. The spectral density matrix $\mathrm{P}_{\mathbf{x}}(f)$ of the M-dimensional array output vector $\mathbf{x}(t)$ can be expressed as

$$\mathrm{P}_{\mathbf{x}}(f) = \mathrm{A}(f,\phi)\mathrm{P}_{\mathbf{s}}(f)\mathrm{A}^H(f,\phi) + \mathrm{P}_{\mathbf{n}}(f) \qquad (1)$$

where $\mathrm{A}(f,\phi) = [\mathbf{a}(f,\phi_1), \mathbf{a}(f,\phi_2), \ldots, \mathbf{a}(f,\phi_d)]$ is the $M \times d$ array steering matrix of the sensor array, $\mathbf{a}(f,\phi_i)$ is the steering vector for the ith source with

DOA ϕ_i, and $\boldsymbol{\phi} = [\phi_1, \ldots, \phi_d]^T$. It is assumed that $M > d$ and that the rank of $\mathrm{A}(f, \boldsymbol{\phi})$ is equal to d at any frequency. The structure of the steering vector $\mathbf{a}(f, \phi)$ changes with the geometry of the array. For a wagon-wheel circular array with five elements, the array steering vector is

$$\mathbf{a}(f_j, \phi) = [e^{-j(2\pi fr/c)\cos\phi}, e^{-j(2\pi fr/c)\sin\phi}, 1, e^{j(2\pi fr/c)\cos\phi}, e^{j(2\pi fr/c)\sin\phi}]^T \tag{2}$$

where r is the radius of the array and c is the speed of sound in air. Here the elements are numbered as 1:East, 2:South, 3:Center, 4:West and 5:North. The DOA is measured wrt North.

The array output vector $\mathbf{x}(t)$ is first decomposed into narrowband components by taking discrete Fourier transform (DFT) over nonoverlapping time segments of length ΔT. That is, the array output $\mathbf{x}(t)$, observed over T_0 seconds, is sectioned into K windows of duration ΔT seconds each. We denote the vector consisting of the jth narrowband components of the independent array measurements at the kth snapshot by $\mathbf{x}_k(f_j)$, $k = 1,2,\ldots,K$, and $j = 1,2,\ldots,J$, and we assume that the narrowband components at different frequency bins are independent. The goal is to determine the number of sources d and estimate the angles ϕ_i, $i = 1,2,\ldots,d$ from the data $\mathbf{x}_k(f_j)$, $k = 1,2,\ldots,K$; $j = 1,2,\ldots,J$.

The spatial covariance matrix for the jth narrowband component $\mathbf{x}_k(f_j)$ is

$$\mathrm{R}_{\mathbf{xx}}(f_j) \approx \mathrm{P}_{\mathbf{x}}(f_j) = \mathrm{A}(f_j, \phi)\mathrm{P}_{\mathbf{s}}(f_j)\mathrm{A}^H(f_j, \phi) + \mathrm{P}_{\mathbf{n}}(f_j), \quad j = 1,2,\ldots,J \tag{3}$$

The spatial covariance $\mathrm{R}_{\mathbf{xx}}(f_j)$ can be approximated from snapshot vectors $\mathbf{x}_k(f_j)$ by averaging across multiple snapshots, i.e.,

$$\mathrm{R}_{\mathbf{xx}}(f_j) = \frac{1}{K}\sum_{k=1}^{K}\mathbf{x}_k(f_j)\mathbf{x}_k^H(f_j). \tag{4}$$

III. WIDEBAND CAPON DOA ESTIMATION METHODS

Several coherent [3, 5, 6, 11] and incoherent [2, 9, 13] wideband DOA estimation algorithms exist that differ in the manner they combine narrowband spectra to provide DOA estimates over a desired frequency range. In coherent frequency combining methods (such as STCM) the narrowband spatial covariance matrices are first focused into a single reference frequency. The focusing process converts the wideband DOA estimation into a narrowband problem where any of the standard narrowband methods may be used to estimate the DOAs. Various weighting schemes [6, 11] can be used to coherently combine the narrowband components. The choice of the focusing matrix has a major impact on the performance of the coherent frequency combining methods. Typically, a diagonal focusing matrix [6, 11] is employed, which can only detect the DOA of a group of closely spaced sources. The spectral content of acoustic signatures of ground vehicles exhibit peaky behavior at certain frequencies where target indications exist, and as a result coherent averaging (particularly in presence of wideband interference) can have detrimental effects on the performance.

In incoherent frequency combining, the spatial covariance matrices are used individually at every frequency to yield separate narrowband responses. Different averaging methods, e.g. arithmetic, harmonic, and geometric averaging, can be employed to incoherently combine the narrowband responses (e.g. see [9]). In the following subsections we introduce different incoherent wideband Capon DOA estimation methods and comment on the advantages and disadvantages of each method.

A. Arithmetic Averaging

In wideband arithmetic Capon beamforming, the goal is to minimize the total output power (across different frequencies) of a set of narrowband beamformers $\mathbf{c}(f_j, \theta)$, $j = 1,\ldots,J$, while enforcing a set of narrowband distortionless response constraints $\mathbf{c}^H(f_j, \theta)\mathbf{a}(f_j, \theta) = 1$, $j = 1,\ldots,J$. The problem can be mathematically posed as

$$\min_{\mathbf{c}(f_j,\theta)} \mathrm{Q}_A(\theta) = \sum_{j=1}^{J}\mathbf{c}^H(f_j, \theta)\mathrm{R}_{\mathbf{xx}}(f_j)\mathbf{c}(f_j, \theta) \tag{5}$$

under the constraints

$$\mathbf{c}^H(f_j, \theta)\mathbf{a}(f_j, \theta) = 1, \qquad \forall \quad j \in [1, J]. \tag{6}$$

This minimization problem can be easily solved using the method of Lagrange multipliers. The minimizers $\mathbf{c}(f_j, \theta)$, $j = 1,\ldots,J$ are narrowband Capon beamformers [4] given by

$$\mathbf{c}(f_j, \theta) = \frac{\mathrm{R}_{\mathbf{xx}}^{-1}(f_j)\mathbf{a}(f_j, \theta)}{\mathbf{a}^H(f_j, \theta)\mathrm{R}_{\mathbf{xx}}^{-1}(f_j)\mathbf{a}(f_j, \theta)}, \qquad \forall \quad j \in [1, J]. \tag{7}$$

The wideband Capon spectrum is given by

$$\mathrm{Q}_A(\theta) = \sum_{j=1}^{J} q(f_j, \theta) = \sum_{j=1}^{J}\frac{1}{\mathbf{a}^H(f_j, \theta)\mathrm{R}_{\mathbf{xx}}^{-1}(f_j)\mathbf{a}(f_j, \theta)} \tag{8}$$

where

$$q(f_j, \theta) = \frac{1}{\mathbf{a}^H(f_j, \theta)\mathrm{R}_{\mathbf{xx}}^{-1}(f_j)\mathbf{a}(f_j, \theta)}, \qquad j = 1,\ldots,J \tag{9}$$

are the output powers of the narrowband Capon beamformers $\mathbf{c}(f_j,\theta)$. It is now clear that the wideband Capon spectrum can be formed by an arithmetic average of the narrowband Capon spectra $q(f_j,\theta)$, $j = 1,\ldots,J$ across different frequency bins.

B. Geometric Averaging

For the wideband geometric Capon beamforming, we minimize the following objective function

$$\mathrm{Q}_G(\theta) = \prod_{j=1}^{J} \mathbf{c}^H(f_j,\theta)\mathrm{R}_{\mathbf{xx}}(f_j)\mathbf{c}(f_j,\theta) \tag{10}$$

with respect to $\mathbf{c}(f_j,\theta)$, $j = 1,\ldots,J$ under the distortionless constraints in (6). The minimizers are again the narrowband Capon beamformers given by (7). Consequently, the wideband Capon spectrum $\mathrm{Q}_G(\theta)$ is given by

$$\mathrm{Q}_G(\theta) = \prod_{j=1}^{J} q(f_j,\theta) = \prod_{j=1}^{J} \frac{1}{\mathbf{a}^H(f_j,\theta)\mathrm{R}_{\mathbf{xx}}^{-1}(f_j)\mathbf{a}(f_j,\theta)} \tag{11}$$

which is the geometric mean of the narrowband Capon spectra across different frequency bins.

C. Harmonic Averaging

Finally, for the harmonically averaged wideband Capon spectrum we have

$$\mathrm{Q}_H(\theta) = \frac{1}{\sum_{j=1}^{J} 1/q(f_j,\theta)} = \frac{1}{\sum_{j=1}^{J} \mathbf{a}^H(f_j,\theta)\mathrm{R}_{\mathbf{xx}}^{-1}(f_j)\mathbf{a}(f_j,\theta)}. \tag{12}$$

Similar to the narrowband case where the DOAs are obtained by searching for the peaks of the Capon spectrum $q(f_j,\theta)$ across θ, in the wideband case the locations of the peaks of $\mathrm{Q}_A(\theta)$ or $\mathrm{Q}_G(\theta)$, or $\mathrm{Q}_H(\theta)$ are taken as the estimate of the DOAs. A prespecified number of peaks can be chosen based on whether or not they reach a threshold which is dependent on the value of the largest peak. The locations of these peaks are the DOA estimates.

D. Wideband Robust Capon Beamformer

In many situations the steering vectors $\mathbf{a}(f_j,\theta)$ are not perfectly known, due to factors such as near field effects, random perturbations in the medium, and uncertainty about the sensor locations. Differences between the presumed steering vectors and the actual ones result in signal suppression and poor interference rejection by the Capon beamformer (e.g. see [14], [16]). Several methods have been reported to make the Capon beamformer robust to such effects. A few examples are: the robust adaptive beamformer of [17], which enforces a white noise gain constraint; robust adaptive beamformer in [12], which considers an ellipsoidal uncertainty for the steering vector; and the robust adaptive beamformer of [18] which optimizes worst case performance for a bounded norm distortion in the steering vector. The reader is referred to [19] for a comprehensive review of the relevant literature.

Our aim in this section is to extend the robust Capon beamforming strategy of [12] for the wideband case. The robust Capon beamforming method in [12] considers an ellipsoidal uncertainty constraint for the steering vector. This method provides a simple way of eliminating the scaling ambiguity. In addition to its good interference cancelation property and robustness to small mismatch in the signal model, it maintains a wide mainlobe for receiving the desired signal.

In [12], it is shown that robust Capon beamforming with ellipsoidal uncertainty constraint is equivalent to solving the following optimization problem under a spherical constraint, i.e.,

$$\min_{\mathbf{a}} \mathbf{a}^H(f_j,\theta)\mathrm{R}_{\mathbf{xx}}^{-1}(f_j)\mathbf{a}(f_j,\theta) \qquad \text{s.t.} \quad \|\mathbf{a}-\bar{\mathbf{a}}\|^2 \le \epsilon \tag{13}$$

where $\bar{\mathbf{a}}(f_j,\theta)$ is the assumed steering vector and ϵ is the error bound. The minimization problem leads to a Capon beamformer with a diagonally loaded covariance matrix. The algorithm requires a 1-D search to find the optimum diagonal loading value at each look direction. The steps for the wideband extension of this algorithm are given below.

1) Compute the singular value decomposition (SVD) of $\mathrm{R}_{\mathbf{xx}}(f_j)$. That is, $\mathrm{R}_{\mathbf{xx}}(f_j) = \mathrm{E}(f_j)\Lambda(f_j)\mathrm{E}^H(f_j)$, where $\Lambda(f_j) = \mathrm{Diag}[\lambda_1,\ldots,\lambda_M]$ contains the eigenvalues with $\lambda_1 \ge \lambda_2 \ge \cdots \ge \lambda_M$ and $\mathrm{E}(f_j)$ is the matrix of all the eigenvectors.

2) Solve for the minimizer of

$$g(\gamma_j) = \sum_{m=1}^{M} \frac{|z_m(f_j)|^2}{(1+\gamma_j\lambda_m)^2} \tag{14}$$

using a 1-D search method (e.g. the Newton's method) and get $g(\gamma_j)$ as close to ϵ as possible. Here γ_j is the diagonal loading factor for frequency f_j, and $z_m(f_j)$ is the mth element of $\mathbf{z}(f_j) = \mathrm{E}^H(f_j)\bar{\mathbf{a}}(f_j,\theta)$.

3) Compute $\mathrm{Q}_G(\theta)$ in (11) for the geometrically averaged output power by replacing $\mathbf{a}(f_j,\theta)$ by

$$\tilde{\mathbf{a}}(f_j,\theta) = \bar{\mathbf{a}}(f_j,\theta) - \mathrm{E}(f_j)(I+\gamma_j\Lambda(f_j))^{-1}\mathrm{E}^H(f_j)\bar{\mathbf{a}}(f_j,\theta). \tag{15}$$

This yields the geometrically averaged robust Capon beamformer in (16)

$$Q_{G_{\text{Robust}}}(\theta) = \prod_{j=1}^{J} \frac{1}{\bar{\mathbf{a}}^H(f_j,\theta)\mathrm{E}(f_j)\Lambda(f_j)[\gamma_j^{-2}I + 2\gamma_j^{-1}\Lambda(f_j) + \Lambda^2(f_j)]^{-1}\mathrm{E}^H(f_j)\bar{\mathbf{a}}(f_j,\theta)}. \tag{16}$$

It is important to note that in addition to a 1-D search, robust wideband Capon beamforming requires an eigen-decomposition of an $M \times M$ Hermitian matrix $R_{\mathbf{xx}}(f_j)$, which has computational complexity $O(M^3)$.

IV. WIDEBAND BEAMSPACE METHOD

The beamspace method reduces the computational complexity and degrees of freedom in an array by steering a group of beams instead of the phasings of the individual sensors [4]. The $M \times M_{bs}$ beamspace matrix B_{bs} is a projection matrix from the element space (in $\mathbb{C}^M$) to the beamspace (in $\mathbb{C}^{M_{bs}}$) where $M \geq M_{bs}$. Finding a covariance with respect to these beams instead of the elements focuses the region of interest (or region of active interference cancellation) and attenuates signals outside this region. The computational complexity is also reduced as the size of the covariance matrix reduces from $M \times M$ to $M_{bs} \times M_{bs}$.

Beamspace method projects the input data vector onto a low dimensional subspace where the signal of interest is extracted easier. This projection cancels signals outside the filtering region of interest, hence acting as a spatial bandpass filter.

In the full-dimensional beamspace, the outputs of the M-element standard array are processed to produce M orthogonal beams. The center beam is typically a conventional (Bartlett window) beam pointed at the look direction, which is called the main response axis (MRA). It is important that the beams are orthogonal, since this ensures that any signal arriving along the mainlobe of a particular beam will not produce output from any other beam. The $M \times M_{bs}$ matrix B_{bs}, ($M_{bs} = M$ for the full-dimensional beamspace), is formed with the steering vectors of each beam, which is called the beamfan. To implement the beamspace method, a beamfan is formed of M_{bs} beams and the MRA is steered to the corresponding look direction. The beamfan is moved through all angles. A general form of a nonorthogonalized beamspace matrix is

$$\mathrm{B}_{no}(f_j,\theta) = [\mathbf{b}(f_j,\phi_{-P}+\theta)\cdots\mathbf{b}(f_j,\phi_0+\theta)\cdots\mathbf{b}(f_j,\phi_P+\theta)] \tag{17}$$

where

$$\mathbf{b}(f_j,\phi_p) = \begin{bmatrix} e^{j2\pi f_j r/c(\alpha_0\cos(\phi_p)+\beta_0\sin(\phi_p))} \\ e^{j2\pi f_j r/c(\alpha_1\cos(\phi_p)+\beta_1\sin(\phi_p))} \\ \vdots \\ e^{j2\pi f_j r/c(\alpha_{M-1}\cos(\phi_p)+\beta_{M-1}\sin(\phi_p))} \end{bmatrix} \tag{18}$$

and ϕ_p, $p = -P,\ldots,0,\ldots,P$ are the angles of beams $\mathbf{b}(f_j,\phi_p)$ in the beamspace matrix measured relative to the x-axis and α_i and β_i are the horizontal and vertical coordinates of the ith sensor relative to the reference position. To ensure orthogonality of the beamspace matrix, we perform

$$\mathrm{B}_{bs} = \mathrm{B}_{no}[\mathrm{B}_{no}^H\mathrm{B}_{no}]^{-1/2} \tag{19}$$

to get $\mathrm{B}_{bs}^H\mathrm{B}_{bs} = I_{M_{bs}}$. The received data is then processed using the beamspace matrix B_{bs} prior to beamforming.

The processing steps in the wideband beamspace method are listed below.

1) Transform the array output vector, $\mathbf{x}_k(f_j)$, $k = 1,2,\ldots,K$ using

$$\mathbf{v}_k(f_j,\theta) = \mathrm{B}_{bs}^H(f_j,\theta)\mathbf{x}_k(f_j) \tag{20}$$

where $\mathrm{B}_{bs}(f_j,\theta)$ is the $M \times M_{bs}$ beamspace matrix whose columns are the orthogonal steering vectors centered around θ at frequency f_j. The resulting sample covariance matrix of the transformed array output, $\mathbf{v}_k(f_j)$ is

$$\begin{aligned} \mathrm{R}_{\mathbf{vv}}(f_j,\theta) &= \mathrm{B}_{bs}^H(f_j,\theta)\mathrm{R}_{\mathbf{xx}}(f_j)\mathrm{B}_{bs}(f_j,\theta) \\ &\approx \mathrm{B}_{bs}^H(f_j,\theta)\mathrm{A}(f_j,\phi)\mathrm{P}_{\mathbf{s}}(f_j)\mathrm{A}^H(f_j,\phi)\mathrm{B}_{bs}(f_j,\theta) \\ &\quad + \mathrm{B}_{bs}^H(f_j,\theta)\mathrm{P}_{\mathbf{n}}(f_j)\mathrm{B}_{bs}(f_j,\theta) \end{aligned} \tag{21}$$

where $A(f_j,\phi)$, $\mathrm{P}_{\mathbf{s}}(f_j)$, and $\mathrm{P}_{\mathbf{n}}(f_j)$ were defined in Section II.

2) The transformed steering vector is given as

$$\mathbf{a}_{bs}(f_j,\theta) = \mathrm{B}_{bs}^H(f_j,\theta)\mathbf{a}(f_j,\theta) \tag{22}$$

and the beamformer output becomes

$$\mathbf{z}_k(f_j,\theta) = \mathbf{c}_{bs}^H(f_j,\theta)\mathbf{v}_k(f_j) \tag{23}$$

where $\mathbf{c}_{bs}(f_j,\theta)$ is

$$\mathbf{c}_{bs}(f_j,\theta) = \frac{\mathrm{R}_{\mathbf{vv}}^{-1}(f_j,\theta)\mathbf{a}_{bs}(f_j,\theta)}{\mathbf{a}_{bs}^H(f_j,\theta)\mathrm{R}_{\mathbf{vv}}^{-1}(f_j,\theta)\mathbf{a}_{bs}(f_j,\theta)}. \tag{24}$$

3) The wideband geometric beamspace spectrum then becomes

$$Q_{G_{bs}}(\theta) = \prod_{j=1}^{J} \frac{1}{\mathbf{a}_{bs}^H(f_j,\theta)\mathrm{R}_{\mathbf{vv}}^{-1}(f_j,\theta)\mathbf{a}_{bs}(f_j,\theta)}. \quad (25)$$

The beamspace method, requires additional computation mostly due to the whitening of the beamspace matrix for each look direction and frequency bin. This can be avoided for the beamspace Capon beamformer by using (19), (21), and (22) in (25) and simplifying the result. This yields a beamspace Capon beamformer that does not need orthogonalization,

$$Q_{G_{bs}}(\theta) = \prod_{j=1}^{J} \frac{1}{\mathbf{a}^H(f_j,\theta)\mathrm{B}_{no}(f_j,\theta)(\mathrm{B}_{no}^H(f_j,\theta)\mathrm{R}_{\mathbf{xx}}(f_j)\mathrm{B}_{no}(f_j,\theta))^{-1}\mathrm{B}_{no}^H(f_j,\theta)\mathbf{a}(f_j,\theta)}. \quad (26)$$

V. BEARING RESPONSE ANALYSIS

Next, we study the bearing response patterns (output power as a function of look angle θ) for the STCM algorithm [5], the arithmetic, geometric, and harmonic wideband Capon beamformers, the wideband robust Capon beamformer, and the wideband beamspace method.

We consider two uncorrelated sources with unit power at angles ϕ_1 and ϕ_2, incident on a five-element wagon wheel array with 2 ft radius. The covariance matrix for the jth narrowband component has rank-2 and is given by

$$\mathrm{R}_{\mathbf{xx}}(f_j) = [\mathbf{a}(f_j,\phi_1)\ \mathbf{a}(f_j,\phi_2)][\mathbf{a}(f_j,\phi_1)\ \mathbf{a}(f_j,\phi_2)]^H. \quad (27)$$

Noise effects with SNR = 20 dB are added to this matrix. We study the resolution of the beamformers mentioned above by analyzing their bearing response pattern for three different angular spacings between the sources: 20°, 23°, and 26°. The set of frequencies used is 50 to 250 Hz with increments of 2 Hz. The reason for using these frequencies is that the aliasing frequency for the wagon-wheel array, is approximately 277 Hz [8], and the useful frequencies of the ground sources lie in this region.

Figs. 1(a)–(f) show the bearing response patterns of the wideband arithmetic mean Capon, geometric mean Capon, harmonic mean Capon, STCM, robust Capon, and beamspace Capon beamformers, respectively. These correspond to the plots of Q_A (arithmetic), Q_G (geometric), Q_H (harmonic), STCM [5], $Q_{G_{\mathrm{robust}}}$ (robust Capon), and $Q_{G_{bs}}$ (beamspace Capon) with respect to look angle θ. Comparing the first four methods, several interesting observations can be made. It can easily be seen from these plots that the width of the mainlobe of the wideband geometric mean is much narrower with a much lower sidelobe (where no source is present) response than the other wideband Capon methods. This is due to the fact that the geometric mean is based upon the product operation where the lower frequencies eliminate any sidelobes, while the higher frequencies narrow the beamwidth and hence giving better overall resolution. On the other hand, the wideband arithmetic and harmonic mean Capon methods exhibit sidelobes that are not observable over the range of angles in Figs. 1(a) and (c). Furthermore, for these methods the resolution does not improve greatly at higher frequencies.

The bearing response of the STCM exhibits a similar mainlobe structure to those of the arithmetic and harmonic mean Capon methods while its sidelobes attenuate more slowly. As can be seen from Fig. 1(e), the wideband robust Capon has problems resolving closely spaced sources when compared with the geometric mean Capon in Fig. 1(b). The beamwidth is dependent on the choice of the diagonal loading parameter in this algorithm, which in turn is determined by the choice of the error bound (ϵ) [12]. The wideband beamspace Capon beamformer used three beams at $-6°$, $0°$, and $6°$ from the look direction. The improvement of the wideband beamspace over the geometric averaged Capon is not noticeable in the bearing responses of Figs. 1(b) and (f), though it indeed acts as a spatial bandpass filter for noise and interference. This advantage of the beamspace Capon algorithm is demonstrated on real data in Section VI.

VI. WIDEBAND DOA ESTIMATION RESULTS

A. Baseline Circular Arrays

In this section, the wideband DOA estimation algorithms developed in this paper are applied to the data of two runs collected using three (nodes 1–3) 5-element wagon-wheel circular arrays each with 2 ft radius. The collected data had to be calibrated prior to DOA estimation using a calibration data set in order to account for the inherent errors between the ideal values of the array parameters, namely microphone gain and phase as well as sensor positions, and the actual values of these parameters for the deployed arrays. The time series recorded

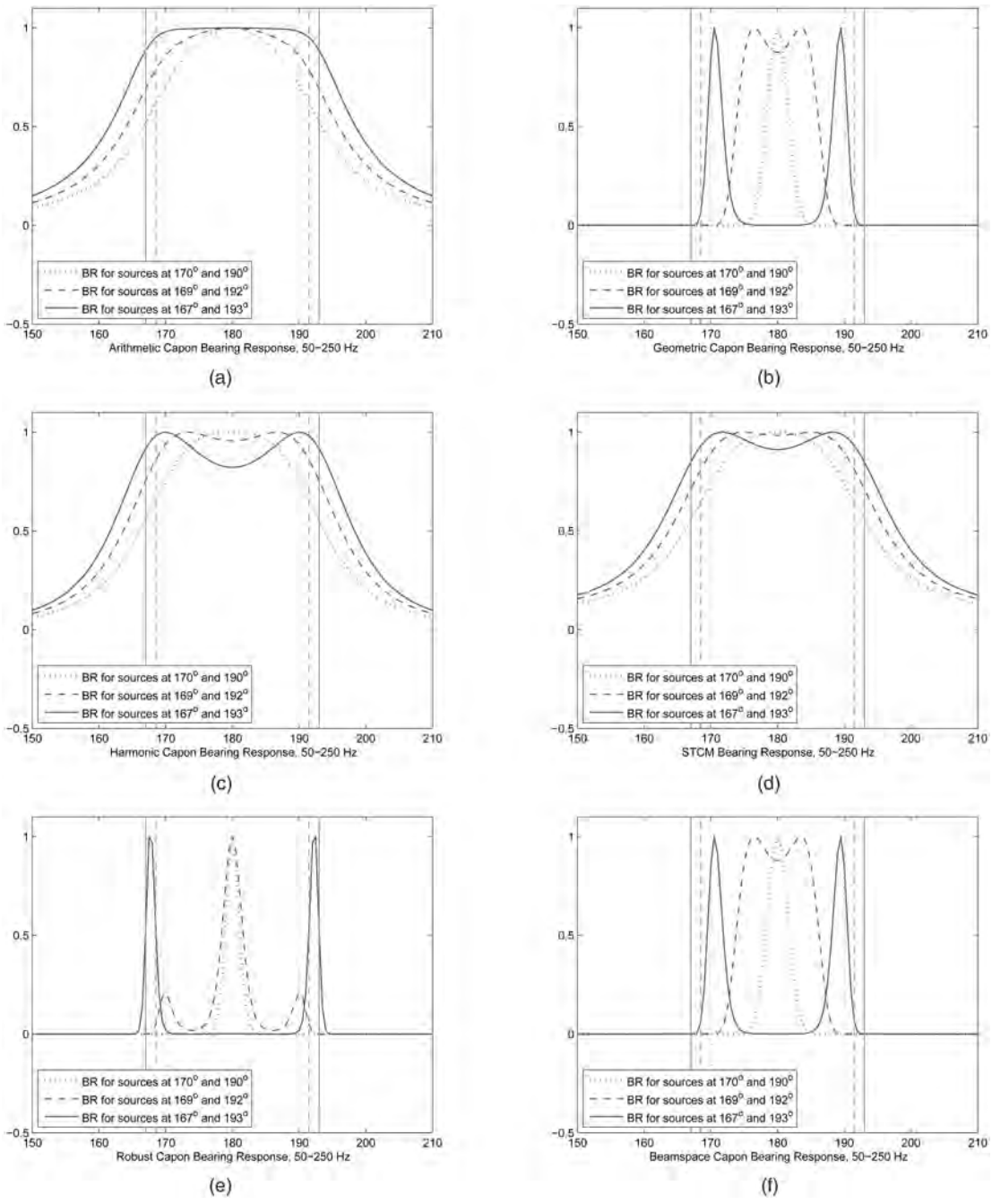

Fig. 1. Bearing responses on 5-element circular array for two sources with separations 20°, 23°, 26°. (a) Arithmetic mean Capon. (b) Geometric mean Capon. (c) Harmonic mean Capon. (d) STCM. (e) Geometric mean robust Capon (with error, $\varepsilon = 0.71$). (f) Geometric mean beamspace Capon. Vertical lines are actual locations of sources.

by each microphone (sampled at f_s = 1024 Hz) was first windowed using a sliding Hamming window of size 2048 that corresponds to 2 sec of data. The overlap between consecutive windows was 1024 sample. The gain/phase calibration process was then performed in the frequency domain in the range of 50–250 Hz using the calibration data set. Due to the overlapping windows the DOA estimation generates DOAs every second. In all the following studies, the beamspace Capon used 3 beams spaced at −6°, 0°, and 6° from the look direction. Moreover, the wideband robust Capon beamformer was applied to the uncalibrated data to show the advantages over the wideband geometric Capon method.

1) *Results on Run 1*: This run contains six vehicles that move in three separate groups. The first group contains a single light wheeled vehicle which started from 1.5 km away, came to 50 m (closest point of approach (CPA)) in the middle of the run, and then moved away to a distance of 2 km from node 1. The second group was formed of a single-file convoy of three heavy tracked vehicles that moved from 2.2 km

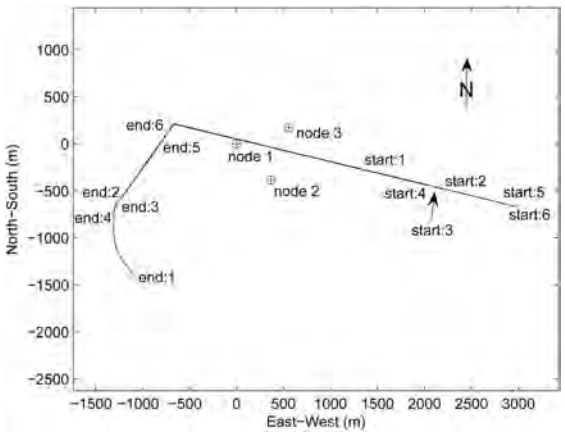

Fig. 2. Vehicle paths on road relative to node positions in run 1.

up to 50 m CPA from the array and moved away to 1.5 km. Lastly, the third group was formed of a single-file convoy of two heavy wheeled vehicles which moved from 3 km into 50 m CPA and then moved away from the array to 0.8 km. The path the vehicles followed relative to the array nodes is shown in Fig. 2. Note that due to page limitations only the results obtained from data for node 1 are presented.

Figs. 3(a)–(e) show the DOA estimation results on the calibrated data for run 1 obtained using the wideband arithmetic Capon, geometric Capon, harmonic Capon, STCM, and beamspace Capon algorithms, respectively. The frequency bin separation was 2 Hz. Solid lines correspond to the actual (true) angles obtained from a truth file. The points marked by "$*$," "$\triangle$," and "$\times$" are the DOA estimates obtained from the first, second, and third strongest peaks in the Capon spectrum, respectively. Comparison of DOA tracks obtained using different algorithms indicates that, among the wideband Capon methods, the geometric and harmonic Capon provide good overall results on run 1 data, with DOA estimates that are close to the actual DOAs. Similar observation was made with other baseline array data sets.

By looking at the DOA estimates and also the range of the vehicles from the array, one can see that the vehicles are accurately resolved even at far ranges (> 2 km). It is interesting to note that although Capon beamforming generally loses its accuracy in presence of near field effects, the DOAs of the vehicles are successfully resolved even when they are near the CPA to the array. It must be mentioned that in some scenarios where both light and heavy vehicles are present together in a run, the dominant source will obscure the weaker source, especially at far ranges.

The arithmetic wideband Capon and the STCM provide acceptable results (Figs. 3(a) and 3(d)), but their DOA estimates are not as accurate as those of the geometric and harmonic Capon beamformers. As can be seen, the geometric and harmonic Capon algorithms have successfully estimated the DOAs of all the groups, even for the light wheeled vehicle at very far range. In particular, the DOA estimates obtained by the geometric and harmonic Capon beamformers for multiple targets between between 150–210 sec and 224–334 sec are very close to the true DOAs. These algorithms are also able to resolve the DOAs of the heavy tracked and wheeled convoy of vehicles moving in single-file groups of three (middle) and two (right hand side) vehicles, respectively. The STCM algorithm on the other hand fails to resolve multiple targets that move in groups, mainly due to its wide beamwidth as shown in Fig. 1(d). Additionally, it fails to provide accurate DOA estimates for the group of three heavy tracked targets as they move away from the array.

The DOA estimation results for the beamspace geometric Capon are shown in Fig. 3(e). Comparing the DOA estimates in the first 110 sec with those obtained by the wideband geometric mean Capon (Fig. 3(b)), we notice that the DOA accuracy has improved, especially when the vehicles are at far range (1.5–2 km). To be more specific, the DOA error during this time segment has reduced from approximately 10° for the wideband geometric mean Capon to less than 5° for the beamspace geometric Capon. This benefit of the beamspace method over the wideband geometric Capon is due to the inherent spatial filtering used in this method. The improvements and benefits of the wideband beamspace Capon method become even more prominent when there are fewer frequency bins to average over, or when the number of samples used to create the covariance matrix is small. In these cases, the beamspace Capon generates better DOA estimates with lower variability due to the inherent robustness to a small number of samples. This property of the beamspace method is a direct consequence of dimension reduction.

To show the sensitivity of the original Capon to phase/gain errors caused by uncertainties in the exact microphone locations and to demonstrate the usefulness of the wideband robust Capon in these cases, the uncalibrated data of run 1 is used. The frequency bin resolution is 4 Hz in this case. The value of the assumed steering vector error is chosen to be $\epsilon = 0.7$. The DOA estimation results of the wideband robust Capon method are shown in Fig. 4(a). Compared with the results of the wideband geometric Capon in Fig. 4(b), the wideband robust geometric Capon provides more accurate DOA estimates. This is especially evident when the targets are near the CPA, i.e., 160–320 s time segment, as can be seen in Figs. 4(c) and (d). This is attributed to the fact that near the CPA, signal mismatch effects due to sensor location errors are compounded by near field effects.

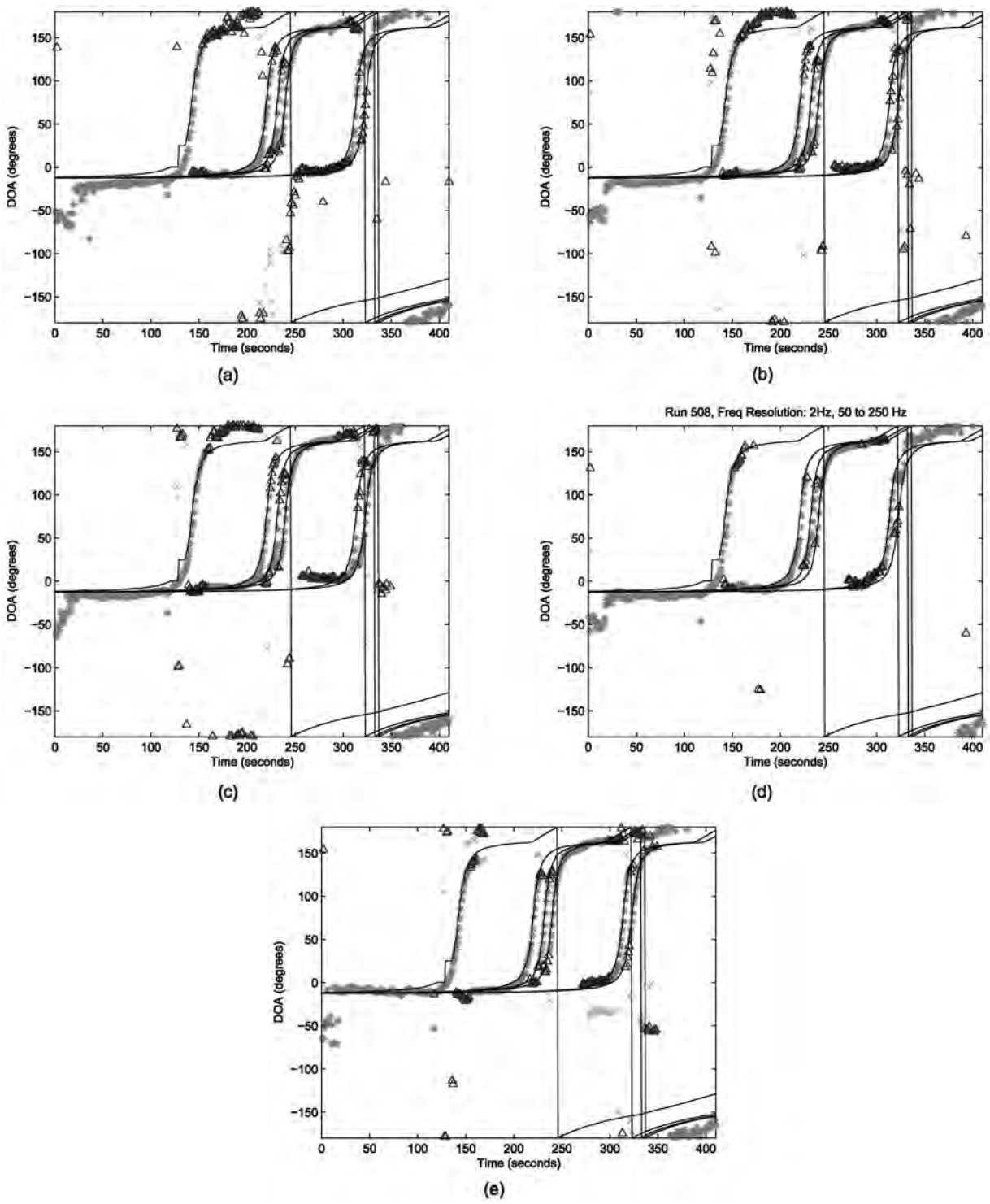

Fig. 3. DOA estimates for run 1 obtained using arithmetic, geometric, harmonic mean wideband Capon. STCM, beamspace Capon algorithms. (a) Arithmetic. (b) Geometric. (c) Harmonic. (d) STCM. (e) Beamspace Capon.

2) *Results on a Single Target Run 2—Accuracy Analysis*: To further benchmark the developed wideband DOA estimation algorithms in terms of DOA estimation accuracy an error analysis is carried out on a single target run. This particular run contains a heavy wheeled vehicle that moves from 1.5 km away to 50 m CPA at approximately 150 s, and then goes away from the array to about 0.75 km. Fig. 5 shows the path of this vehicle on the road relative to array locations.

Figs. 6(a)–(e) show the DOA estimation results on this single-target run obtained using the arithmetic mean Capon, the geometric mean Capon, the harmonic mean Capon, STCM, and the geometric beamspace Capon algorithms, respectively. DOA estimates obtained by using a conventional

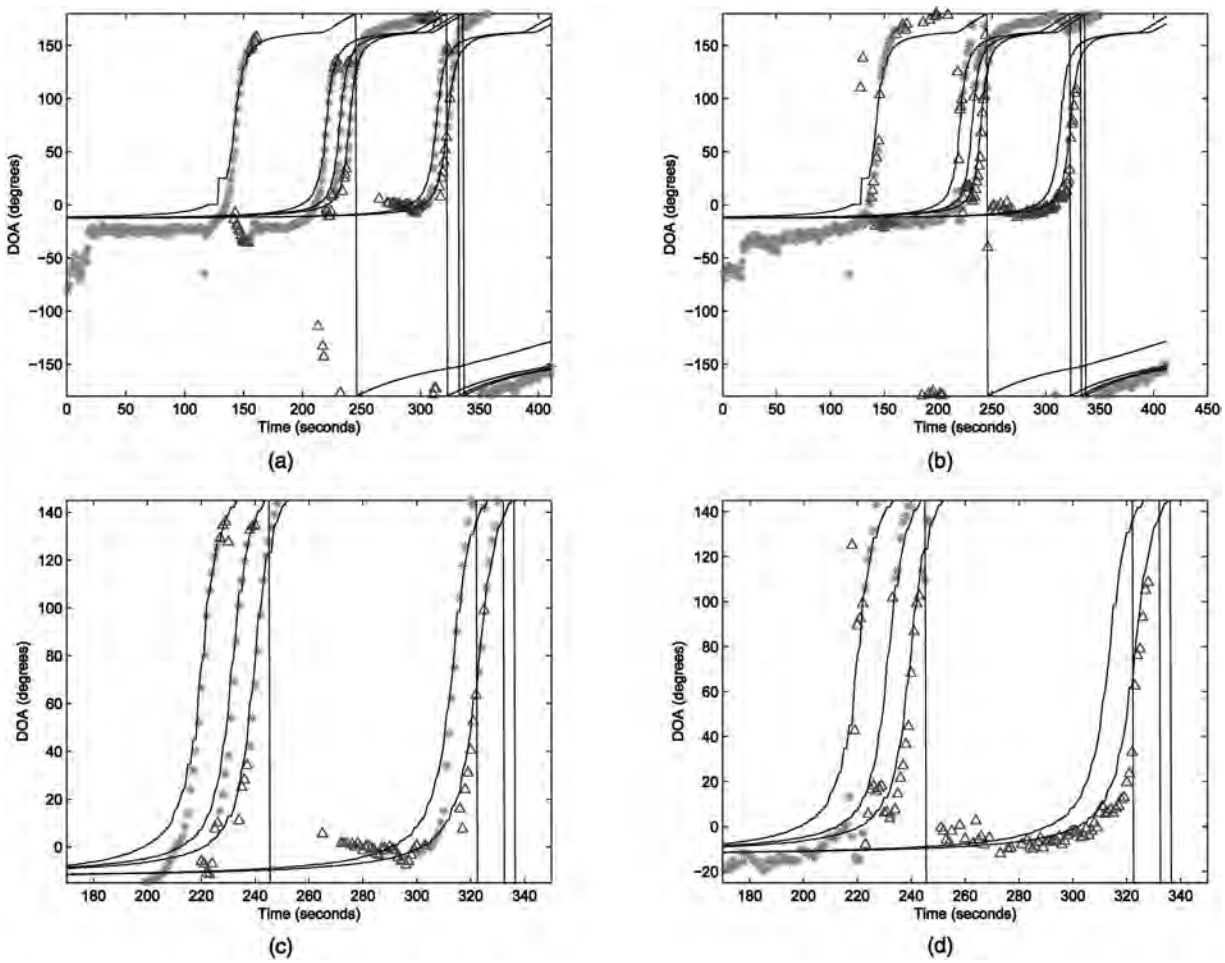

Fig. 4. DOA estimates of wideband robust Capon ($\varepsilon = 1.5$) and geometric mean Capon. For uncalibrated data of run 1, (a) and (b). Near field DOA estimation performance, (c) and (d).

Fourier-based (Bartlett) beamformer [4] are also provided for comparison. Fig. 6(f) shows that the large sidelobes of the conventional Fourier beamformer cause many erroneous DOA estimates. The distributions of the DOA errors are shown in Fig. 7. The mean and variance of the error are also given in Table I. As evident from these results, the beamspace Capon algorithm provided the most accurate (smallest variance) DOA estimates. The improved accuracy is due, in part, to the spatial filtering property of the beamspace method.

B. Randomly Distributed Arrays

To show some additional promising properties of the beamspace Capon algorithm a separate study is carried out using random distributed wireless sensors. Distributed sensor arrays offer numerous benefits compared with arrays with regular geometries. These include: simplicity and ease in deployment, stealthy operation, larger coverage area, better spatial resolution for separating multiple closely spaced targets, lower hardware complexity and cost, etc. We have recently shown [20] that distributed sensor arrays offer much better robustness to sensor position errors, transmission loss effects, and other perturbations. This is primarily due to random sidelobe structure in contrast to the regular sidelobe structure of the baseline wagon-wheel arrays. To see this, let us consider the sensor array configuration in Fig. 8(b), consisting of fifteen randomly distributed sensors. Figs. 9(a) and (b) show the theoretical bearing response patterns of the wideband geometric

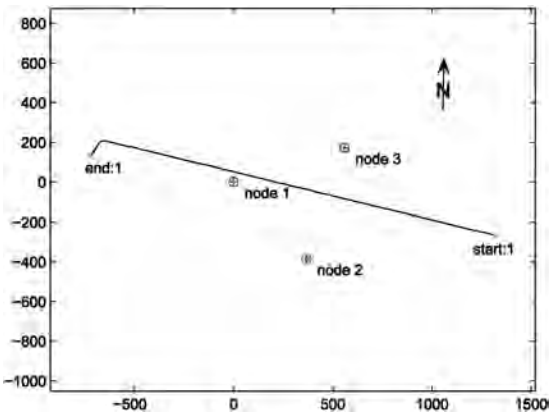

Fig. 5. Vehicle paths on road relative to node positions—run 2.

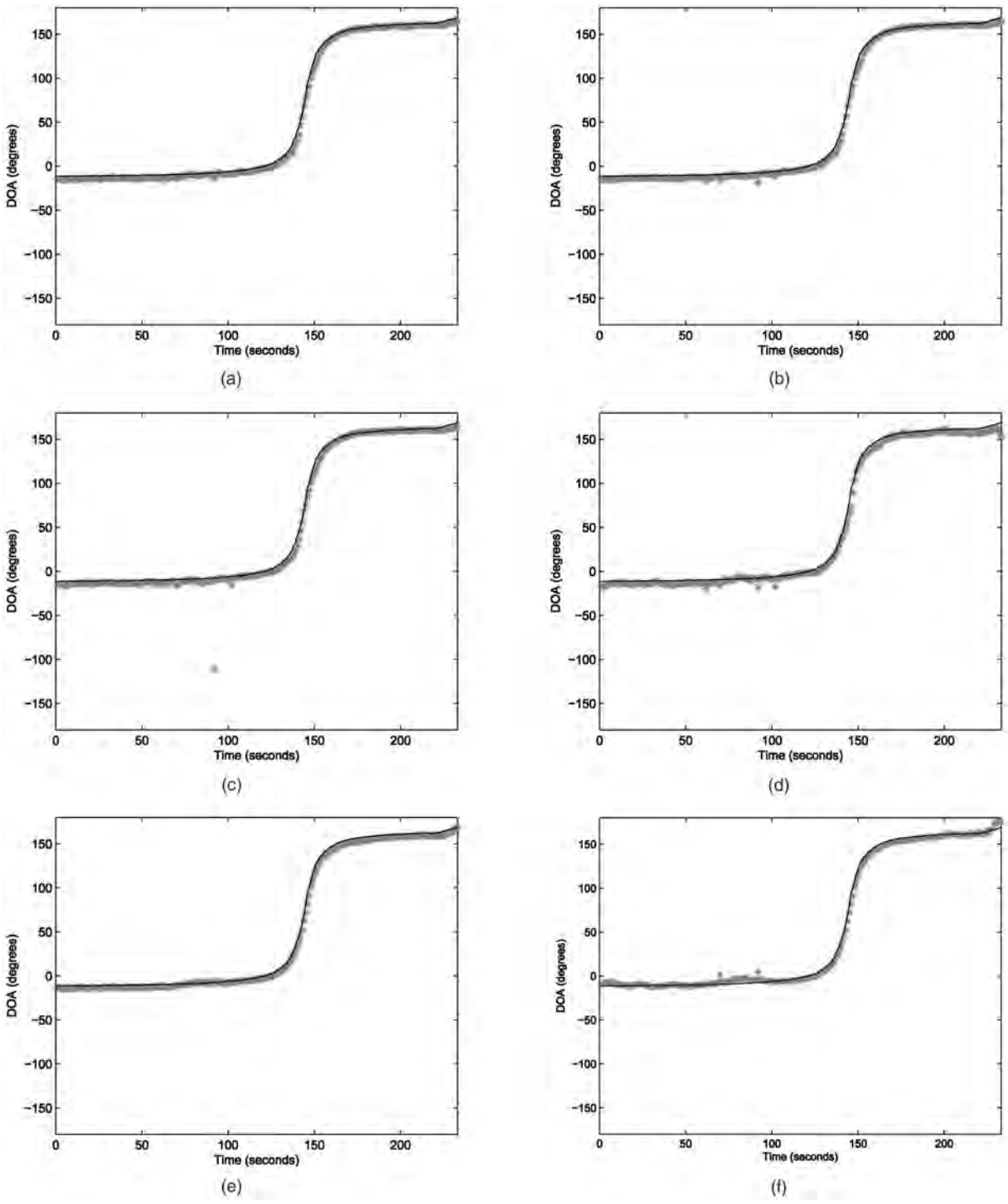

Fig. 6. DOA estimates for run 2, a single target case, obtained using arithmetic, geometric, harmonic mean wideband Capon, STCM, beamspace Capon, conventional beamforming algorithms. (a) Arithmetic Capon. (b) Geometric Capon. (c) Harmonic Capon. (d) STCM. (e) Beamspace Capon. (f) Conventional.

Capon and the wideband beamspace Capon, respectively. The frequency resolution in this study was 8 Hz and the SNR was 20 dB (similar to the baseline case). As expected the bearing response patterns for the randomly distributed arrays exhibit better resolution for separating closely spaced (2 deg separation) sources with no regular sidelobe structure compared to those in Figs. 1(b) and (f) for the baseline array. Nonetheless, in distributed sensor arrays sensor failures and/or packet losses commonly occur, causing incorrect DOA estimation and target localization. We show that the wideband geometric beamspace method is robust with respect to such failures.

Data sets have been collected using two wireless sensor array configurations in Figs. 8(a) and (b).

TABLE I
DOA Error Statistics for Various Wideband Beamforming Algorithms

	Beamspace	Geometric	Arithmetic	STCM	Harmonic	Conventional
Mean Error (deg)	−1.5685	−2.1239	−2.201	−.9299	−1.2134	−0.6913
Variance of Error (deg)	2.0621	3.2046	3.9177	5.0255	9.0960	8.9530
No. of outliers ($\|error\| > 10°$)	0	0	0	2	1	2

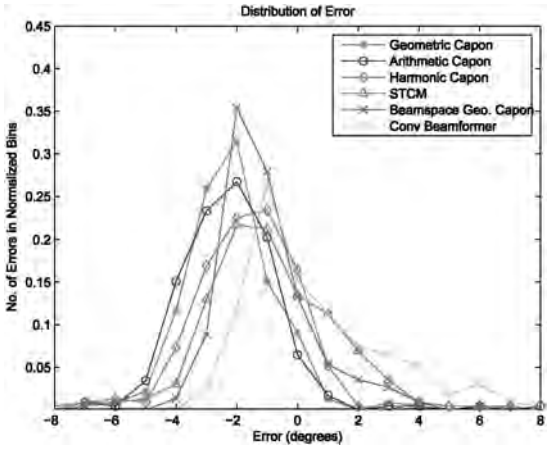

Fig. 7. Error distributions for single target run.

For each configuration, fifteen mote-based (Zigbee compliant) sensors were randomly distributed within a 25 m radius area. Configuration II, which contains tight and sparse sensor clusters, offers better spatial and frequency diversity; while configuration I offers better separation of closely spaced vehicles due to more uniform spreading of the sensors. The sensor locations were obtained using a relatively accurate GPS unit to within an average error radius of 0.1 m. The worst case localization error radius was around 0.25 m for some sensors. Data were collected for various runs using either single or two light wheeled diesel trucks. The recorded data of each sensor was sampled at f_s = 1024 Hz. All 15 sensors transmit, in real-time, the stream of synchronized recorded time series in a single hop to a base station while the vehicles move in the field. The collected data sets were used not only to show the real potential of the distributed sensors for acoustic DOA trajectory estimation of the vehicles but also to evaluate the empirical performance of the wideband geometric Capon and the wideband beamspace Capon algorithms for scenarios where data transmitted to the base station was lost or unreliable.

During the data collection some sensors failed to collect reliable data because of either bad microphone, or amplifier circuit, or both. To account for sensor failure in the DOA estimation process, one has to screen the data and manually remove the failed data channels before beamforming. This precludes real-time DOA estimation. To demonstrate the usefulness of the wideband beamspace method in these situations, this method is employed here without using the knowledge of the failed sensors or their number. In other words the data from failed sensors is included for beamforming. The wideband beamspace preprocessing allows the beamforming to proceed normally and provides excellent results even in the presence of multiple failed data channels.

Fig. 10(a) shows the results for a run with one failed sensor using the wideband geometric mean Capon beamformer. As can be seen, when the failed data channel is not removed the DOA estimates vary significantly with a large number of spurious estimates and poor angular trajectory estimate of the vehicle.

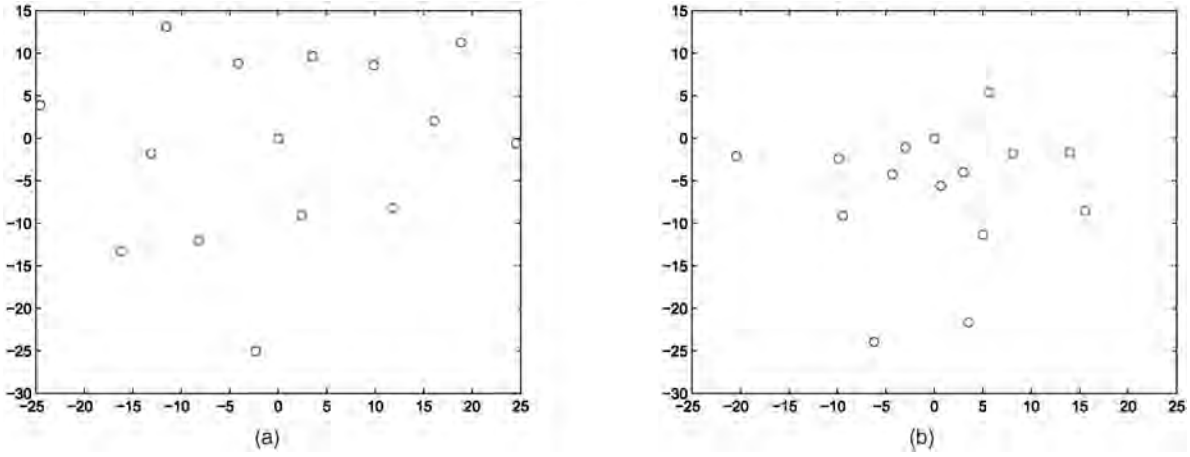

Fig. 8. Two randomly distributed sensor configurations using 15 mote-based sensors. (a) Configuration I. (b) Configuration II.

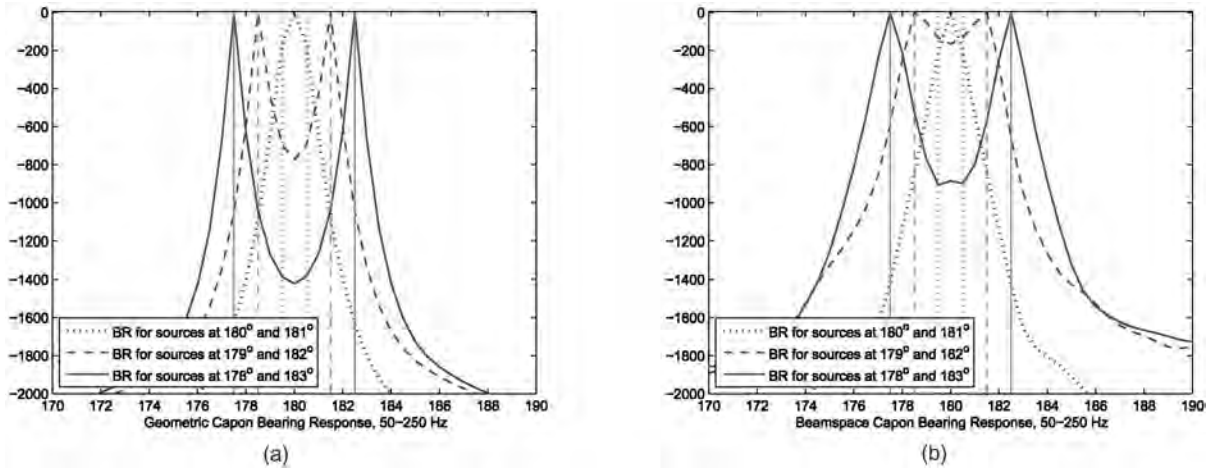

Fig. 9. Bearing response patterns obtained for 15-element randomly distributed array observing two sources with angular separations of 1°, 3°, 5°. (a) Wideband geometric Capon. (b) Wideband geometric beamspace Capon.

Fig. 10(c) shows the results of this algorithm after manually removing the failed data channel. Clearly, removing the bad data restored the accuracy of DOA estimation hence providing a reasonably clear vehicle trajectory estimate. Fig. 10(e), on the other hand, shows the results when using the wideband beamspace Capon beamformer. We notice that the beamspace preprocessing leads to significant improvement in the angular trajectory estimate of the vehicle without the need to identify and remove the failed sensor data. Figs. 10(b), (d), and (f) show the DOA estimates of these algorithms for a run with two sensor failures. The results in Fig. 10(b) obtained using the wideband geometric mean Capon beamformer is completely unreliable in this case. The improvement that the beamspace preprocessing method offers over the wideband geometric mean Capon beamformer is clearly noticeable. The wideband beamspace does not provide accurate DOA estimates in the time segment 90–105 s. This may be attributed to the fact that at near field the number of sensor failures has an increasingly detrimental effect on the ability of the array to provide accurate DOA estimation.

An explanation for the beamspace robustness to sensor failure is the inherent complex weighting of the sensor element inputs in such a way that it only relies on a subset of the sensors in the array. This would not normally prevent errors in the beamforming when a regular geometry array is used. However, because of the random distributed configuration and the angular focusing of the beamspace method, the inputs from the failed sensors add only small errors into the steering vector. In contrast, the wideband geometric Capon beamformer performs interference cancelation over the entire angular field of view, and hence receives the full effect of the failed sensors.

VII. CONCLUSIONS

Three wideband Capon beamforming methods were introduced for estimating the DOAs of multiple closely spaced moving sources with wideband acoustic signatures. The proposed methods exploit different incoherent averaging operations, namely arithmetic, geometric, and harmonic averaging, of a set of narrowband Capon spectra. A wideband robust Capon beamformer was also developed to robustify the algorithms with respect to array calibration errors and near field effects. In addition, the beamspace method was extended to the wideband case to improve the resolution of DOA estimation and to offer robustness with respect to sensor failures.

A study was carried out to benchmark these different wideband Capon methods in terms of their beamwidth, DOA accuracy, and effectiveness in presence of sensor failures. The results suggest the superiority of the geometric mean Capon beamformer and the wideband beamspace extension in terms of the ability to provide accurate DOA estimates. Although the wideband beamspace method did not provide substantially better results on the multiple target run, it greatly reduced the variance of the DOA estimate error. The results on baseline run 1 also indicated better performance of this method at far ranges when the sources are hard to detect. When used in conjunction with distributed sensor arrays the wideband beamspace algorithm was found to be robust to sensor data failures. The robust geometric Capon provided better results on the uncalibrated data when compared with those of the wideband geometric mean Capon beamformer. This was especially prevalent in near CPA situations where the effects of sensor location errors are compounded by the near field effects.

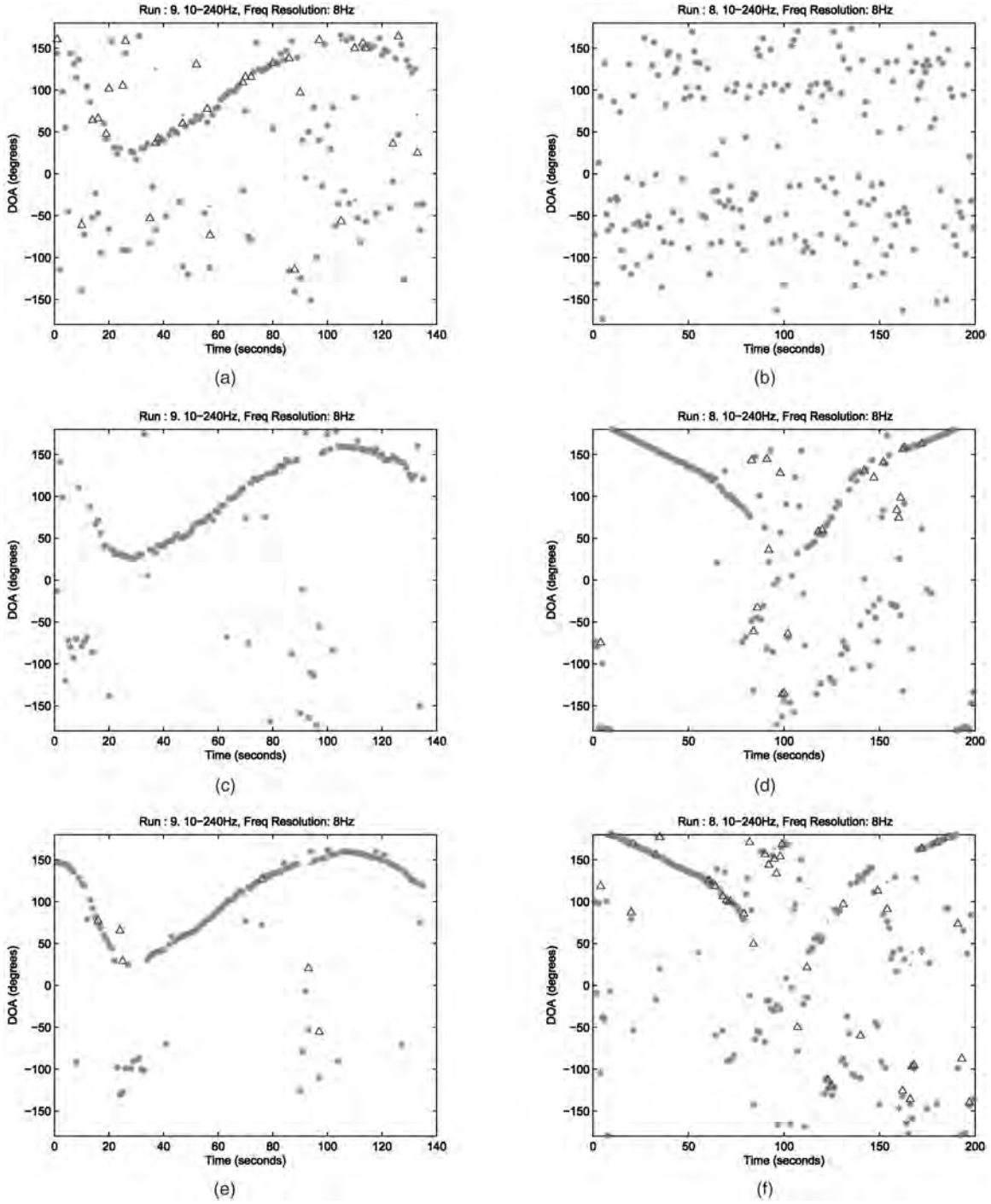

Fig. 10. Comparison of wideband geometric Capon beamforming and wideband geometric Capon with beamspace preprocessing when one or two sensor failures occur. Run 2 collected using configuration I, run 1 collected using configuration II (a) Wideband geometric mean Capon beamformer—run 1. (b) Wideband geometric mean Capon beamformer—run 2. (c) Wideband geometric mean Capon beamforming—run 1 failed sensor removed. (d) Wideband geometric Capon beamforming—run 2 failed sensors removed. (e) Wideband beamspace Capon—run 1. (f) Wideband beamspace Capon—run 2.

MAHMOOD R. AZIMI-SADJADI
Information System Technologies, Inc.
Fort Collins, CO 80521
E-mail: (mo@infsyst.biz)

NICHOLAS ROSEVEARE
ALI PEZESHKI
Dept. of Electrical and Computer Engineering
Colorado State University
Fort Collins, CO 80523

REFERENCES

[1] Srour, N.
Unattended ground sensors—A prospective for operational needs and requirements.
ARL Report Prepared for NATO, Oct. 1999.

[2] Pham, T., and Fong, M.
Real-time implementation of MUSIC for wideband acoustic detection and tracking.
Proceedings of SPIE AeroSense'97: Automatic Target Recognition VII, Orlando, FL, Apr. 1997.

[3] Pham, T., and Sadler, B. M.
Wideband array processing algorithms for acoustic tracking of ground vehicles.
ARL Technical Report, Adelphi, MD, 1997.

[4] Van Trees, H. L.
Optimum Array Processing.
New York: Wiley Interscience, 2002.

[5] Krolik, J.
Focused wideband array processing for spatial spectral estimation.
In S. Haykin (Ed.), *Advances in Spectrum Analysis and Array Processing, Vol. II*, Upper Saddle River, NJ: Prentice-Hall, 1991.

[6] Wang, H., and Kaveh, M.
Coherent signal subspace processing for the detection and estimation of angles of arrival of multiple wideband sources.
IEEE Transactions on Acoustics, Speech and Signal Processing, **33** (1985), 823–831.

[7] Damarla, T. R.
Tracking a convoy of multiple targets using acoustic sensor data.
Proceedings of SPIE—Acquisition, Tracking, and Pointing XVII, vol. 5082, Aug. 2003, 37–42.

[8] Hohil, M. E., Heberley, J. R., Chang, J., and Rotolo, A.
Vehicle counting and classification algorithms for unattended ground sensors.
Proceedings of SPIE-Unattended Ground Sensor Technologies and Applications V, vol. 5090, Sept. 2003, 99–110.

[9] Azimi-Sadjadi, M. R., Pezeshki, A., Scharf, L., and Hohil, M.
Wideband DOA estimation algorithms for multiple target detection and tracking using unattended acoustic sensors.
Proceedings of the SPIE'04 Defense and Security Symposium, Unattended Ground Sensors VI, vol. 5417, Apr. 2004, 1–11.

[10] Di Claudio, E. D., and Parisi, R.
WAVES: Weighted average of signal subspaces for robust wideband direction finding.
IEEE Transactions on Signal Processing, **49**, 10 (2001), 2179–2191.

[11] Hung, H., and Kaveh, M.
Focusing matrices for coherent signal subspace processing.
IEEE Transactions on Acoustics, Speech and Signal Processing, **36** (1988), 1272–1281.

[12] Li, J., Stoica, P., and Wang, Z.
On robust capon beamforming and diagonal loading.
IEEE Transactions on Signal Processing, **51** (July 2003), 1702–1715.

[13] Azimi-Sadjadi, M. R., and Roseveare, N.
Capon beamspace beamforming for distributed acoustic arrays.
Proceedings of SPIE'07 Defense and Security Symposium, vol. 6562, Apr. 2007.

[14] Cox, H.
Resolving power and sensitivity to mismatch of optimum array processors.
Journal of the Acoustical Society of America, **54** (1973), 771–758.

[15] Feldman, D. D., and Griffiths, L. J.
A projection approach to robust adaptive beamforming.
IEEE Transactions on Signal Processing, **42** (Apr. 1994), 867–876.

[16] Reed, I. S., Mallett, J. D., and Brennan, L. E.
Rapid convergence rate in adaptive arrays.
IEEE Transactions on Aerospace and Electronic Systems, **AES-10** (Nov. 1974), 853–863.

[17] Cox, H., Zeskind, R. M., and Owen, M. H.
Robust adaptive beamforming.
IEEE Transactions on Acoustics, Speech, Signal Processing, **ASSP-35** (Oct. 1987), 1365–1376.

[18] Vorobyov, S. A., Gershman, A. B., and Luo, Z.-Q.
Robust adaptive beamforming using worst-case performance optimization: A solution to the signal mismatch problem.
IEEE Transactions on Signal Processing, **51** (Feb. 2003), 313–324.

[19] Li, J., and Stoica, P.
Robust Adaptive Beamforming.
New York: Wiley, 2005.

[20] Azimi-Sadjadi, M. R., Jiang, Y., and Wichern, G.
Properties of randomly distributed sparse acoustic sensors for ground vehicle tracking and localization.
Proceedings of SPIE'06 Defense and Security Symposium, vol. 6201, Apr. 2006.

A LOS Rate Estimation Method for Bank-to-Turn Missiles

We compensate for the effect of the fast roll motion of bank-to-turn (BTT) missiles through appropriate coordinate transformation. Thereby, the proposed line-of-sight (LOS) rate estimator can provide better estimation performance than the previously known passive target tracking methods since it is independent of seeker-stabilization loop and robust with the measurement noise.

I. INTRODUCTION

Most well-known guidance laws need the accurate information of line-of-sight (LOS) rate for their successful implementation. Since LOS rate cannot be measured directly, it is usually estimated from some other measurable quantities based on the dynamic model of LOS rate. Unfortunately, it is not an easy problem to design a good LOS rate estimator because

Manuscript received February 8, 2007; revised September 21, 2007; released for publication March 27, 2008.

IEEE Log No. T-AES/44/4/930743.

Refereeing of this contribution was handled by Y. Oshman.

This research was supported by the Defense Acquisition Program Administration and Agency for Defense Development, Korea, through the Image Information Research Center at Korea Advanced Institute of Science & Technology under Contract UD070007AD.